Performance of a Novel Miniature Antenna Implanted in the Human Head for Wireless Biotelemetry

Asimina Kiourti*, Maria Christopoulou and Konstantina S. Nikita
School of Electrical & Computer Engineering
National Technical University of Athens
Athens, Greece
akiourti@biosim.ntua.gr, mchrist@biosim.ntua.gr, knikita@cc.ece.ntua.gr

***Abstract*—In this study, we present a novel, miniaturized, biocompatible antenna at the medical implant communications service (MICS) band (402–405 MHz) for integration in wireless biotelemetry devices implanted in the human head. To reduce simulation time, the antenna is designed while in the center of a skin tissue simulating box and subsequently implanted inside the skin tissue of an anatomical human head model. The resonance, radiation and specific absorption rate (SAR) performance of the antenna is evaluated and design modifications are suggested to overcome the inherent detuning effect.**

Keywords-Biocompatibility; finite difference time domain (FDTD); implantable antenna; medical implant communications service (MICS) band; specific absorption rate (SAR); wireless biotelemetry

I. INTRODUCTION

Wireless biotelemetry between implanted devices and exterior monitoring/control equipment has recently drawn great attention for diagnosis and therapy [1]. In the past, implanted devices relied on induction between two coils for communication [2], [3]. Due to the low exhibited data rates, restricted range of communication and sensitivity to coils' misalignments, research is now oriented towards the design of implant–integrated antennas. In the most common scenario, signals are wirelessly transmitted at the medical implant communication service (MICS) band of 402–405 MHz [4].

Several implantable antennas have been proposed in the literature both for generic ([5]–[7]) and application–specific (physiological parameter monitoring [8], user location tracking [9], medical data transmission in a sickroom [10]) biotelemetry. Antennas implanted in the human head have also been investigated. A planar inverted–F antenna (PIFA) designed for intracranial pressure (ICP) monitoring at 2.45 GHz is presented in [11]. In [12], the communication performance of a MICS loop antenna placed under the scalp is characterized, while in [13], a comparative analysis is performed for head–implanted loop and short dipole antennas at several frequency bands.

In this paper, a novel MICS PIFA is proposed for skin tissue implantation. Simulations are carried out with the finite difference time domain (FDTD) method. Evaluation of the antenna implanted inside the skin tissue of an anatomical human head model is performed. Significant size reduction is achieved compared to previously reported implantable MICS antennas, while emphasis is given on the biocompatibility and market–availability of the materials. Bandwidth enhancement, quality of the communication with an exterior antenna and Specific Absorption Rate (SAR) conformance with the IEEE C95.1–1999 [14] and IEEE C95.1–2005 [15] basic restrictions are also taken into account. Although head implantation is studied (e.g. integration in ICP monitors, brain wave sensors for paralyzed patients, trackers of persons with Alzheimer's disease etc.), the antenna can also be used for several other wireless biotelemetry applications.

The paper is organized as follows. Section II presents the design of the proposed antenna. In Section III, FDTD simulation results are provided. In Section IV, design modifications are suggested to correct antenna detuning. The paper concludes in Section V.

II. ANTENNA DESIGN

The proposed antenna is an improved version of the one presented in [16]. Biocompatible alumina (ε_r = 9.4, tanδ = 0.06), which has long been used in medical implants [17], is now selected as the dielectric material, and sheet thicknesses which are available in the market are utilized.

The design is shown in Fig. 1(a)–(d). The antenna consists of a circular ground plane (R_1 = 4 mm) and two vertically–stacked, circular, meandered radiating patches (R_2 = 3.9 mm). The center of the ground plane is set as the origin of the coordinate system throughout this study, according to Fig. 1. Each of the radiating patches is printed on an 0.25 mm–thick alumina substrate, while an 0.15 mm–thick alumina superstrate layer covers the structure to preserve its biocompatibility and robustness. Round shape is preferred to avoid vertexes that could cause tissue injuries. A 50 Ohm coaxial cable (x = 0 mm, y = 3 mm) feeds both radiating patches, while a 0.2 mm–radius shorting pin (x = 3 mm, y = –1 mm) connects the ground plane with the lower patch to achieve a further reduction in size. The width of the meanders equals 0.5 mm, and their lengths are given in Table 1. Numbers start at the top (feed point location) and increase to the bottom of each patch.

The proposed antenna achieves a significant size reduction compared to previously reported implantable MICS antennas, as indicated in Table II.

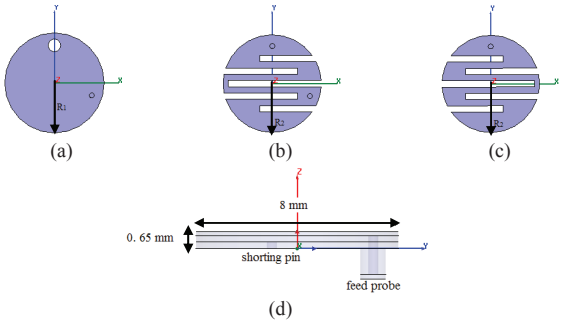

Figure 1. Design of the proposed implantable antenna: (a) ground plane, (b) lower patch, (c) upper patch, and (d) side view.

TABLE I. MEANDER LENGTHS

Meander #	Length [mm]	
	Lower patch	*Upper patch*
1	4.485	4.485
2	5.827	5.827
3	7.392	7.392
4	5.827	5.827
5	4.485	4.485

TABLE II. SIZE COMPARISON WITH LITERATURE

Antenna	Volume occupied [mm^3]
[1]	$24 \times 32 \times 4 = 3072$
[7]	$22.5 \times 18.5 \times 1.9 = 790.9$
[8]	$23 \times 23 \times 1.25 \approx 661.3$
[18]	$\pi \times 7.5^2 \times 1.9 \approx 335.76$
[5]	$\pi \times 5^2 \times 1.815 \approx 142.6$
[6]	$8 \times 8 \times 1.9 = 121.6$
proposed	$\pi \times 4^2 \times 0.65 \approx 32.7$

III. RESULTS

FDTD simulations are conducted in XFDTD [19]. To reduce simulation time, the antenna is designed while in the center of the 100 mm–edge cubic skin tissue simulating box of Fig. 2(a) [16]. The antenna is subsequently implanted inside the skin tissue of a 13–biological tissue anatomical human head model, as illustrated in Fig. 2(b). Free–space surrounds both setups by 200 mm ($\lambda_0/4 \approx 186.5$ mm, where λ_0 is the free–space wavelength at 402 MHz). Cells of $0.1 \times 0.1 \times 0.05$ mm^3, $2.5 \times 2.5 \times 2.5$ mm^3, $1.25 \times 1.25 \times 1.25$ mm^3 and $10 \times 10 \times 10$ mm^3 are used for the antenna, skin box, head model and free–space, respectively. Meshing is adaptive to avoid abrupt transitions. Extensive validation checks have been carried out through comparison with Finite Element Method (FEM) simulations.

Table III summarizes the permittivity (ε_r) and conductivity (σ) values of the tissues used in the simulations at 402 MHz [20]. Moreover, the maximum deviation of the ε_r and σ values in the frequency range 300–500 MHz from their values at 402 MHz is recorded. The deviations are small enough, indicating that the tissues' dielectric properties can approximately be considered as frequency–independent inside a small frequency range. The mass density of the tissues is also provided.

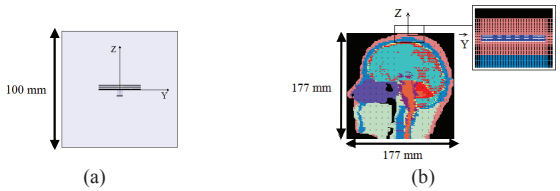

Figure 2. Simulation setup of the antenna implanted inside (a) a skin-tissue simulating box and (b) the skin tissue of an anatomical human head model.

TABLE III. ELECTRIC PROPERTIES AT 402 MHZ, MAXIMUM DEVIATION FROM THE 402 MHZ VALUES IN THE 300–500 MHZ RANGE AND MASS DENSITY OF THE TISSUES USED IN THE SIMULATIONS

Tissue	ε_r	σ [S/m]	$\Delta\varepsilon_r$ [%]	$\Delta\sigma$ [%]	Mass Density [kg/m^3]
Skin (Dry)	46.74	0.69	6.59	7.25	1100
Bone (Cortical)	13.14	0.09	2.28	11.11	2200
Dura	46.65	0.83	7.87	3.61	1100
Cerebrospinal Fluid	70.97	2.25	2.48	1.33	1020
Brain Grey Matter	57.40	0.74	4.56	6.76	1030
Brain White Matter	42.05	0.45	4.11	8.89	1030
Muscle	57.11	0.80	1.91	3.75	1040
Cartilage	45.45	0.59	2.90	6.78	1100
Vitreous Humor	69.00	1.53	0.03	0.65	1000
Lens	48.14	0.67	1.68	2.99	1100
Eye Sclera	57.66	1.00	2.15	2.00	1100
Spinal Cord	35.39	0.45	4.29	6.67	1040
Cerebellum	55.94	1.03	6.74	5.83	1030

A. *Resonance Characteristics*

The simulated return loss and input impedance (Z_{in}) frequency responses of the antenna are shown in Fig. 3 and Fig. 4, respectively. For comparison reasons, both simulation setups of Fig. 2 are considered. The antenna is designed to resonate at 402 MHz while in the skin tissue simulating box, with a broad bandwidth of 40 MHz (defined at a return loss less than –10 dB). Implantation of the antenna in the skin tissue of the anatomical human head model shifts its resonance frequency to 413 MHz and reduces its bandwidth to 38 MHz. These can be attributed to the change in the loading effect of the surrounding tissues and the exterior air on the antenna. Despite the inherent detuning, a satisfactory return loss of –30.4 dB ($Z_{in} = 51.9 - j\,2.4$ Ohms) and –14.9 dB ($Z_{in} = 55.2 + j\,18.6$ Ohms) is achieved at the desired frequency of 402 MHz for the simulation setups of Fig. 2(a) and (b), respectively.

B. *Radiation Performance*

The far–field gain radiation pattern of the proposed antenna at 402 MHz is depicted in Fig. 5 for both implantation scenarios of Fig. 2. Since the antenna is electrically very small, it radiates an omni–directional radiation pattern while in the center of the skin tissue simulating box (Fig. 5(a)). Implanting the antenna in the skin tissue of the anatomical human head model modifies its loading and alters its electrical size and radiation pattern (Fig. 5(b)). A relatively good radiation efficiency (radiated to net input power ratio) of 0.81% (e.g. [1], [6]) is obtained for the antenna in this simulation setup.

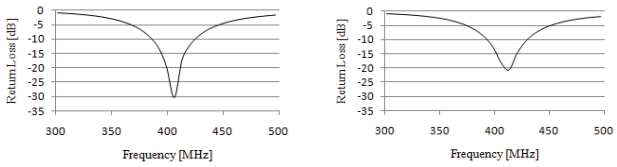

(a) (b)

Figure 3. Return loss frequency response of the proposed antenna for the simulation setups of (a) Fig. 2(a) and (b) Fig. 2(b).

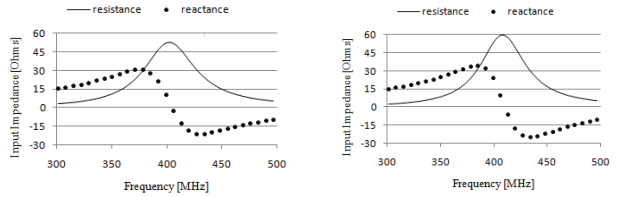

(a) (b)

Figure 4. Input impedance frequency response of the proposed antenna for the simulation setups of (a) Fig. 2(a) and (b) Fig. 2(b).

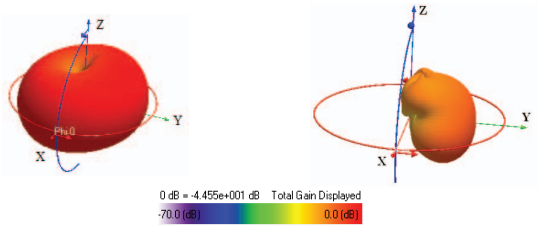

(a) (b)

Figure 5. Far–field gain radiation pattern of the proposed antenna at 402 MHz for the simulation setups of (a) Fig. 2(a) and (b) Fig. 2(b).

C. *SAR Restrictions and Distribution for the Anatomical Human Head Model Simulation Setup*

Assessing the electromagnetic power absorbed by the tissues which surround the antenna inside the anatomical human head model is a critical issue. For this purpose, an SAR numerical analysis is performed at 402 MHz for the antenna simulation setup of Fig. 2(b). A net input power of 1 W is initially assumed and the peak 1–g averaged (1–g avg) and 10–g averaged (10–g avg) SAR values are mentioned in Table IV. To conform with the IEEE C95.1–1999 (1–g avg SAR < 1.6 W/kg [14]) and IEEE C95.1–2005 (10–g avg SAR < 2 W/kg [15]) basic restrictions for general public exposure, the actual net input power of the antenna should not exceed the values of Table V. The IEEE C95.1–1999 standard is found to be stricter, limiting the maximum allowed net input power of the antenna to a value more than ten times lower than that imposed by the IEEE C95.1–2005 standard.

The distributions of the local SAR are shown in Fig. 6, for the slices where maximum local SAR value has been calculated. To satisfy the strictest limitations set by the IEEE guidelines, the net input power has been set equal to 2.35 mW. According to the radiation efficiency (0.81%) of the antenna, such a net input power will generate a radiated power of about 19 μW, which satisfies the limitation for the effective radiated power (ERP) (25 μW in free space [21]). For comparison reasons, all SAR results have been normalized to 2 W/kg.

TABLE IV. PEAK 1–G AND 10–G AVG SAR VALUES FOR THE ANTENNA IMPLANTED INSIDE THE ANATOMICAL HUMAN HEAD MODEL (NET INPUT POWER 1 W)

Simulation Setup	peak 1–g avg SAR [W/kg]	peak 10–g avg SAR [W/kg]
anatomical human head model (Fig. 2(b))	679.79	82.02

TABLE V. MAXIMUM ALLOWED NET INPUT POWER FOR THE ANTENNA IMPLANTED INSIDE THE ANATOMICAL HUMAN HEAD MODEL TO CONFORM WITH THE IEEE BASIC RESTRICTIONS

	maximum allowed net input power [mW]	
Simulation Setup	***IEEE C95.1–1999***	***IEEE C95.1–2005***
anatomical human head model (Fig. 2(b))	2.35	24.38

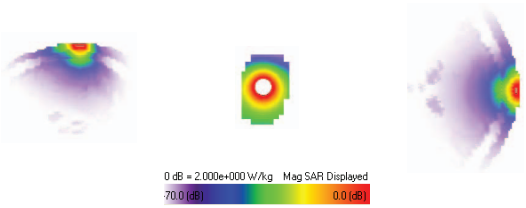

(a) (b) (c)

Figure 6. Distribution of the local SAR on the (a) yz, (b) xy, and c) xz slices of the simulation setup of Fig. 2(b) where maximum local SAR has been calculated (net input power 2.35 mW).

D. *Communication Performance for the Anatomical Human Head Model Simulation Setup*

Since the antenna will be integrated in a wireless biotelemetry device implanted inside the human head, the performance of its communication with an exterior monitoring/control device needs to be assessed. For this purpose, the simulation setup of Fig. 7(a) is considered. The proposed antenna is implanted according to the scenario of Fig. 2(b) and acts as a transmitter (Tx). For simplicity reasons, the receiving antenna (Rx) is assumed to be a half–wavelength ($\lambda_0/2 \approx 373.14$ mm, where λ_0 is the free–space wavelength at 402 MHz) dipole antenna. The Rx is placed horizontally above the Tx and symmetrically around the z–axis, so that the centers of the antennas are aligned.

Moving the Rx from 5 mm to 200 mm horizontally along the z–axis, thus increasing the Tx–Rx separation distance, the coupling between the antennas is recorded in terms of the coupling coefficient, $|S_{21}|$. Simulation results are shown in Fig. 7(b). The coupling coefficient, $|S_{21}|$, quantifies power transmission in the wireless link, so that $|S_{21}|^2 = P_r/P_t$, where P_t is the available power at the Tx, and P_r is the power delivered to a 50 Ohm load terminating the Rx [11]. To satisfy the strictest limitations set by the IEEE guidelines for the SAR, the net input power of the antenna is set to 2.35 mW (see Table V), which corresponds to P_t = 2.43 mW (≈ 3.86 dBm). The dependence of P_r on the Tx–Rx distance is shown in Fig. 7(c). A large variation is observed in coupling strength, and thus power received, with distance. Assuming the most distal scenario of this study, the exterior receiver should have enough sensitivity to detect the signal from the implanted device which is as weak as –56.2 dBm.

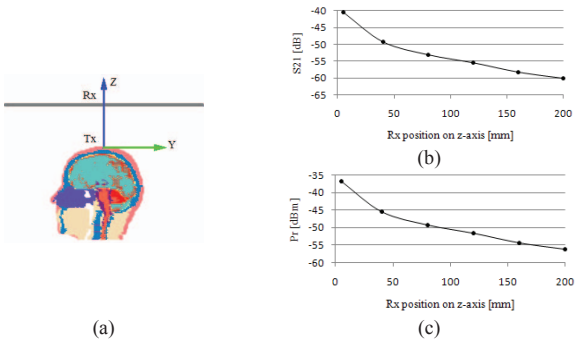

Figure 7. (a) Simulation setup to assess the antenna's communication performance, and simulated (b) $|S_{21}|$ and (c) P_r (P_t = 3.86 dBm) versus Rx position on the z–axis.

IV. Suggestions for Antenna Detuning Correction

Correcting the detuning effect discussed in Fig. 3 can improve the antenna's performance. Regarding the simulation setup of Fig. 2(b), shifting the antenna's resonance frequency from 413 MHz down to 402 MHz requires an increase in its current flow length. This could be performed in a number of ways, the most obvious being lengthening of the meanders and re–positioning of the shorting pin. For example, increasing the length of meanders 1 and 5 of both patches to 4.985 mm tunes the antenna at 402 MHz with a return loss of –23.3 dB. Keeping the meander lengths unchanged and re–positioning the shorting pin to x = –0.5 mm, y = –1.5 mm tunes the antenna at 402 MHz with a return loss of –17 dB. Several other design modifications can be suggested to re–tune the antenna inside the anatomical human head model. Therefore, the best practice is to design the antenna inside the skin tissue simulating box, where simulations run fast, and perform re–tuning corrections on the last stage of the design.

V. Conclusion and Future Work

A novel miniature PIFA was presented for integration in a wireless MICS biotelemetry device implanted in the human head. To reduce simulation time, the design was performed while the antenna was placed in the center of a skin tissue simulating box. Subsequent implanting of the antenna inside the skin tissue of an anatomical human head model resulted in only a minor detuning effect. The antenna's resonance and radiation characteristics were evaluated and its maximum allowed net input power was calculated to conform with the IEEE C95.1–1999 and C95.1–2005 basic restrictions for general public exposure. Finally, the quality of communication between the proposed antenna and an exterior $\lambda_0/2$ dipole antenna was assessed and design modifications were suggested to correct the inherent detuning effect.

Future work will include evaluation of the communication performance between the proposed antenna and sophisticated exterior antennas to suit specific application requirements. Furthermore, optimization algorithms will be applied to the antenna implanted inside the anatomical head model to optimally correct the detuning effect. Subsequent investigations will also include construction of the proposed antenna and experimental validation of the simulation results.

References

[1] J. Kim and Y. Rahmat-Samii, "Implanted antennas inside a human body: simulations, designs and characterizations," IEEE Trans. Microw. Theory Tech., vol. 52, pp. 1934–1943, Aug. 2004.

[2] W. G. Scanlon, N. E. Evans, and J. B. Burns, "FDTD analysis of closed-coupled 4-18 MHz radiating devices for human biotelemetry," Phys. Med. Biol., vol. 44, pp. 335–345, 1999.

[3] G. C. Crumley, N. E. Evans, J. B. Burns, and T. G. Trouton, "On the design and assessment of a 2.45 GHz radio telecommand system for remote patient monitoring," Med. Eng. Phys., vol. 20, pp. 750–755, Mar. 1999.

[4] "Medical implant communications service (MICS) federal register," Rules Reg., vol. 64, no. 240, pp. 69926–69934, Dec. 1999.

[5] W. C. Liu, S. H. Chen, and C. M. Wu, "Implantable broadband circular stacked PIFA antenna for biotelemetry communication," J. of Electromagn. Waves and Appl., vol. 22, pp. 1791–1800, 2008.

[6] W. C. Liu, S. H. Chen, and C. M. Wu, "Bandwidth enhancement and size reduction of an implantable PIFA antenna for biotelemetry devices," Microw. Opt. Technol. Lett., vol. 51, pp. 755–757, Mar. 2009.

[7] C. M. Lee, T. C. Yo, F. J. Huand, and C. H. Luo, "Bandwidth enhancement of planar inverted-F antenna for implantable biotelemetry," Microw. Opt. Technol. Lett., vol. 51, pp. 749–752, Mar. 2009.

[8] T. Karacolak, R. Cooper, and E. Topsakal, "Electrical properties of rat skin and design of implantable antennas for medical wireless telemetry," IEEE Trans. Antennas Propag., vol. 57, pp. 2806–2812, Sept. 2009.

[9] M. Z. Azad and M. Ali, "A miniature implanted inverted-F antenna for GPS application," IEEE Trans. Antennas Propag., vol. 57, pp. 1854–1858, Jun. 2009.

[10] W. Xia, K. Saito, M. Takahashi, and K. Ito, "Performances of an implanted cavity slot antenna embedded in the human arm," IEEE Trans. Antennas Propag., vol. 57, pp. 894–899, Apr. 2009.

[11] R. Warty, M. R. Tofighi, U. Kawoos, A. Rosen, "Characterization of implantable antennas for intracranial pressure monitoring: reflection by and transmission through a scalp phantom," IEEE Trans. Microw. Theory Tech., vol. 56, pp. 2366–2376, Oct. 2008.

[12] Z. N. Chen, G. C. Liu, and T. S. P. See, "Transmission of RF signals between MICS loop antennas in free space and implanted in the human head," IEEE Trans. Antennas Propag., vol. 57, pp. 1850–1853, Jun. 2009.

[13] C. A. Roopnariane, M. R. Tofighi, and C. M. Collins, "Radiation performance of small implanted antennas in head at MICS, ISM, and GPS bands," in Proc. IEEE 36th Annu. Northeast Bioeng. Conf., New York, NY, pp. 1–2, Mar. 2010.

[14] "IEEE Standard for Safety Levels with Respect to Human Exposure to Radio Frequency Electromagnetic Fields, 3kHz to 300GHz," IEEE Standard C95.1–1999, 1999.

[15] "IEEE Standard for Safety Levels with Respect to Human Exposure to Radio Frequency Electromagnetic Fields, 3kHz to 300GHz," IEEE Standard C95.1–2005, 2005.

[16] A. Kiourti, M. Christopoulou, S. Koulouridis, and K. S. Nikita, "Design of a novel miniaturized implantable PIFA for biomedical telemetry," in Proc. ICST Int. Conf. Wireless Mobile Commun. Healthcare, in press.

[17] W. W. Capello, J. D'Anthonio, J. Feinberg, and M. Manley, "Alternative Bearing Surfaces: Alumina Ceramic Bearings for Total Hip Arthroplasty," in Bioceramics and Alternative Bearings in Joint Arthroplasty, Session 3, Eds. Springer, 2005, pp. 87–94.

[18] V. M. Lee, T. C. Yo, and C. H. Luo, "Compact broadband stacked implantable antenna for biotelemetry with medical devices," in Proc. IEEE Annu. Wireless Microw. Tech. Conf., Clearwater Beach, FL, pp. 1–4, Dec. 2006.

[19] XFDTD, Electromagnetic Solver Based on the Finite Difference Time Domain Method, Remcom Inc.

[20] C. Gabriel, S. Gabriel, and E. Corthout, "The dielectric properties of biological tissues," Phys. Med. Biol., vol. 41, pp. 2231–2293, 1996.

[21] "ERC recommendation 70–03 relating to the use of short range devices (SRD)," in Proc. Of Eur. Postal Telecommunications Administration Conf., CEPT/ERC 70–03, Annex 12, Tromso, Norway, 1997.